

Research Article

Cite this article: Qiu J, Shen Bf, Zhang LG, Zhang XM, Huang S, Cao LH, Yu W (2018). Generation of collimated electron jets from plasma under applied electromagnetostatic field. *Laser and Particle Beams* **36**, 384–390. <https://doi.org/10.1017/S0263034618000381>

Received: 15 May 2018

Revised: 14 August 2018

Accepted: 23 August 2018

Key words:

Applied electromagnetostatic field; electron jets; energy gain; PIC simulation; plasma

Author for correspondence:

Baifei Shen and Xiaomei Zhang, State Key Laboratory of High Field Laser Physics, Shanghai Institute of Optics and Fine Mechanics, Chinese Academy of Sciences, Shanghai 201800, China.
E-mail: bfshen@mail.shcnc.ac.cn; zhxm@siom.ac.cn

Generation of collimated electron jets from plasma under applied electromagnetostatic field

Jing Qiu^{1,2}, Baifei Shen^{1,3}, Lingang Zhang¹, Xiaomei Zhang¹, Shan Huang^{1,2}, Lihua Cao^{4,5} and Wei Yu¹

¹State Key Laboratory of High Field Laser Physics, Shanghai Institute of Optics and Fine Mechanics, Chinese Academy of Sciences, Shanghai 201800, China; ²University of Chinese Academy of Sciences, Beijing 100049, China; ³Department of Physics, Shanghai Normal University, Shanghai 200234, China; ⁴Institute of Applied Physics and Computational Mathematics, Beijing 100088, China and ⁵HEDPS, Center for Applied Physics and Technology Peking University, Beijing 100871, China

Abstract

The collimated electron jets ejected from cylindrical plasma are produced in particle-in-cell simulation under the applied longitudinal magnetostatic field and radial electrostatic field, which is a process that can be conveniently performed in a laboratory. We find that the applied magnetostatic field contributes significantly to the jet collimation, whereas the applied electrostatic field plays a vital role in the jet formation. The generation mechanism of collimated jets can be well understood through energy gain of the tagged electrons, and we conclude that the longitudinal momentum of the electrons is converted from the transverse momentum via the transverse-induced magnetic field. It has been found that the ejecting velocity of the jets is close to the speed of light when the applied electrostatic field reaches 3×10^{10} V/m. The present scheme may also give us an insight into the formation of astrophysical jets in celestial bodies.

Introduction

Electron jets (Chen *et al.*, 2002; Hu *et al.*, 2010), which are collimated outflows from plasma, have potential applications as a compact source of high-energy-density relativistic electrons (Yu *et al.*, 2015). The electron flows have been widely studied based on the conventional accelerator and laser-driven plasma acceleration (Katsouleas and Dawson, 1983; Nakajima *et al.*, 1995, 2015; Sprangle *et al.*, 1996; Wagner *et al.*, 1997; Yu *et al.*, 2000; Salamin and Keitel, 2002), especially in direct laser acceleration (Gahn *et al.*, 1999; Shaw *et al.*, 2014, 2017), and laser-driven wakefield acceleration (Ting *et al.*, 1997; Nakajima *et al.*, 2011; Zhang *et al.*, 2012; Albert *et al.*, 2014; Salehi *et al.*, 2017; Woodbury *et al.*, 2018) schemes. In the conventional accelerator, which is usually of a large scale due to the limited acceleration gradient, charged particles are injected into the electric field and gain energy directly from this acceleration field. In laser-driven plasma acceleration, which can be a relatively compact system, both accelerated charged particles and quasi-neutral plasma flows (Kang *et al.*, 2016) can be obtained from plasma driven by the high-frequency electromagnetic field. Here, instead of the laser as the driver, we propose a very different method of obtaining the collimated axial electron jets from the cylindrical plasma in the presence of inward radial electrostatic field and axial magnetostatic field. According to the well-known cross-field plasma rotating effect (Wilcox, 1959; Baker *et al.*, 1961; Fahleson, 1961; Lehnert, 1971), the motion of the non-relativistic charged particles can be described as a superposition of three simple motions: a uniform rectilinear drift velocity (Baker *et al.*, 1961) given by $\vec{E} \times \vec{B} / B^2$ leading to the rotation of the plasma, a cyclotron motion about an axis parallel to the magnetic field, and a uniform rectilinear velocity in the direction of the magnetic field. Among the three kinds of velocities, only the first is determined by the fields while the others are closely related to the instantaneous fields, which is produced by the interaction of the applied electromagnetostatic field with plasma. Under the applied electromagnetostatic field, the electrons move spirally toward the center of the cylindrical plasma in the transverse plane. Considering the high density of the electrons in the center, the electrons are expected to eject out from the plasma. Here we should note that the jets could be found under the *Z*-pinch effect (Haines, 2011; Zhai *et al.*, 2014), resulting from the radial Lorentz force, which originates from the intense current in the axial direction. While jets are generated in both *Z*-pinches and our cases, the mechanism is different. The experiments of rotating plasma (Wilcox, 1959; Baker *et al.*, 1961; Fahleson, 1961; Lehnert, 1971) have been carried out in the laboratory. With similar structure of axial magnetic field and radial electric field as that in our proposal, the phenomenon of electron

rotating is both observed. With the electric field and magnetic field in 10^8 V/m and 10 T scale, respectively, which are far higher than that in the previous experiments where the jets have not been observed, we found electron jets from our performed particle-in-cell (PIC) simulations and gave the qualitative explanation of the jet formation. With similar setup in the rotating plasma device (Fahleson, 1961), our proposed model could be achieved in the laboratory when the applied electric field is matched. In our scheme, the coaxial disc-annulus electrode is set along the axis of the cylindrical plasma to produce a radial electrostatic field, which would accelerate the electrons into the center and induce the electron jets. Meanwhile, the axial magnetostatic field is set to collimate the electrons (Bridle, 1986; Zhai *et al.*, 2014; Wang *et al.*, 2016). The plasma is set as cold state initially, to avoid the effect of the initial temperature of the plasma on the electron jet formation, since the initial temperature of the plasma is conducive to the electron jet formation. (With the plasma of a temperature $T = 1$ keV at time $t = 0$ ps, the electron jets with better collimation and higher intensity shown in online Supplementary Figure S1d–1f are achieved than that with the plasma in the cold state at $t = 0$ ps, shown in online Supplementary Figure S1a–1c, respectively.) The collimated plasma jet could be formed on the plasma focus device (Kasperczuk *et al.*, 2016, 2017), where the conical geometry contributes to the jet formation. Considering the simplification configuration of the system, the plasma in our simulations is cylindrical. (The cubic configuration is also simulated and the electron jets have also been observed.) The absorbed boundary conditions for both fields and particles are set in the simulation. Under the absorbed boundary conditions, the fields transmit totally through the boundary, and the particles are omitted when they contact the boundary material. As is well known, axial magnetic fields exist in celestial bodies, and radial electric fields will be formed owing to the rapid expansions or contractions of the celestial bodies. As the structure of these electric and magnetic fields may be similar to that in our proposed model, the jets observed in celestial bodies may be somewhat related to our model.

In this paper, the validity of the model is confirmed through full three-dimensional PIC simulations in the millimeter scale based on VORPAL (Nieter and Cary, 2004). Under the application of proper electrostatic and magnetostatic field parameters, electrons eject out from the plasma to form collimated jets, which are perpendicular to the applied electrostatic field. Compared with the jets formed without the application of a magnetostatic field, the jets in the present model is better collimated, as the applied magnetostatic field contributes considerably to the jet collimation. The electric field is found to play a vital role in the jet formation process, according to the distinct distributions of the transverse and longitudinal energy gains of all electrons. Moreover, the ejecting velocity of the jets is close to the speed of light, when the applied electrostatic field reaches 3×10^{10} V/m.

Simulations and discussions

PIC simulation

In our model, the x direction is noted as the longitudinal direction whereas the yz plane is in the transverse direction. The anode, which is on the axis of the cylindrical cold plasma, has infinite length and uniform charge distribution. According to Gauss'

law, the radial electric field E_r is obtained as below

$$E_r = \begin{cases} E_{\max} \times r/r_0 & r \leq r_0 \\ E_{\max} \times r_0/r & r_0 < r \leq R_0 \end{cases}, \quad (1)$$

where $r = \sqrt{y^2 + z^2}$. The radii of the anode and plasma are $r_0 = 10^{-2}R_0$ and $R_0 = 3.0$ mm, respectively. The cold plasma with the density $n_0 = 1.3 \times 10^{14}$ cm $^{-3}$ is initially located in the region of -0.5 mm $\leq x \leq 0.5$ mm, $\sqrt{y^2 + z^2} \leq R_0$. For simplicity, we assign $E_{\max} = q_l/(2\pi\epsilon_0 r_0)$, in which q_l is the amount of charge per unit length and ϵ_0 is the dielectric constant of vacuum. In the simulation, $E_{\max} = 3 \times 10^8$ V/m and the applied longitudinal uniform magnetic field $B_0 = 11$ T. The simulation box is in the range of -1.0 mm $\leq y, z \leq 1.0$ mm and -3.1 mm $\leq y, z \leq 3.1$ mm, corresponding to a window with $250 \times 250 \times 250$ cells containing five particles per cell. Under the effect of the applied electrostatic and magnetostatic fields, the electron flows eject from both ends of the cylindrical plasma symmetrically and in opposite directions, as illustrated clearly in Figure 1.

Illustration of the model results

The simulation results in Figure 1 clearly show that the longitudinal electron momentum P_x manifests the formation of the jets. Under the effect of the applied electrostatic and magnetostatic fields, the electrons move toward the center of the cylindrical plasma along spiral tracks. Two spiral lines denote the tracks of two typical electrons e_1 and e_2 ejecting along the $+x$ and $-x$ directions, respectively, as shown in Figure 1. Their color variations from blue to red indicate the time lapse from 0 to 20 ps. During this period, some electrons are ejected out from the plasma in the longitudinal direction with spiral motion in the transverse direction (also shown in Fig. 2a). Here we should note that some other electrons are ejected away from the plasma in the longitudinal direction with little transverse motion because of their initial localization with intense electric field, whereas others remain in the plasma because of their initial localization with weak electric field.

As shown in Figure 1, the jet is well collimated, when compared with that under the same condition but without the applied magnetostatic field (shown in Fig. S2), which indicates that the applied magnetostatic field is of great significance in the jet collimation process. The motion of the electrons at $x = 0.25$ mm in the presence of the applied magnetostatic field $B_0 = 11$ T is displayed in Figure 2a and the equivalent motion when $B_0 = 0$ T is displayed in Figure 2b. Here only the transverse velocity of the electron is considered. In the case of $B_0 = 0$ T, the electrons are accelerated directly into the plasma center and later disperse in the transverse direction. The electrons experience very different motion while in the presence of the applied magnetostatic field. They move spirally in the transverse plane as shown clearly in Figure 2a, which leads to the collimation of the jets. Here we note that the direction of the force imposed on the electrons initially is transverse, but eventually they gain longitudinal velocity and some of them eject from the plasma. The induced electric field (IEF) and the induced magnetic field (IMF) play important roles in the electron jet formation, which will be discussed below.

IEF and IMF

At time $t = 2$ ps, the longitudinal current and IEF are already formed as shown in Figure 3a and 3d, respectively. The IEF E_x

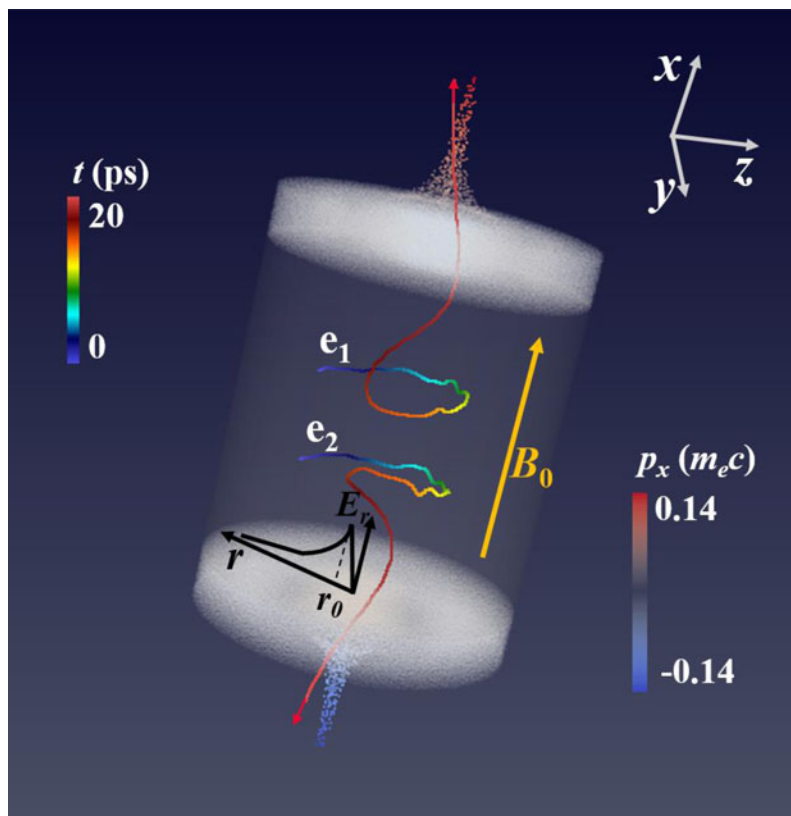


Fig. 1. Simulation results of the jet model. Electron jets are clearly seen at the two ends of the cylindrical plasma, which is shown from the higher longitudinal electron momentum P_x at time $t = 20$ ps, where the origin of the coordinate is at the plasma center. The applied uniform magnetostatic field is $B_0 = 11$ T in the x direction, and the maximum of the applied radial electrostatic field is $E_{\max} = 3 \times 10^8$ V/m. For a clear demonstration of the tracked localization of electrons, the middle part is left empty to show the tracks of two typical electrons e_1 (0.22, -0.19 , 0.016 mm) and e_2 (-0.17 , -0.19 , 0.016 mm) from time $t = 0$ ps to $t = 20$ ps. The tracks are shown as curved lines colored from blue (cold) to red (warm), respectively.

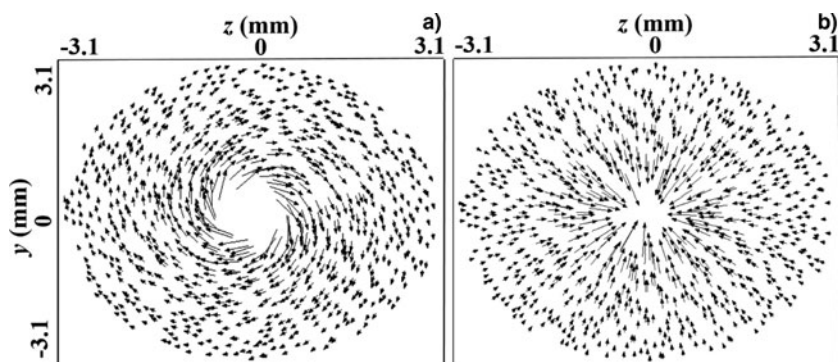


Fig. 2. Transverse velocity vectors of the electrons in the yz plane of $r \geq 0.5$ mm (chosen for clear demonstration) at $x = 0.25$ mm (within the plasma) when $t = 2$ ps (a) with the applied magnetostatic field and (b) without the applied magnetostatic field.

is formed at $x = \pm 0.5$ mm around the center of the yz plane, as shown in Figure 3d; it is conducive to accelerate the electrons to form the currents in Figure 3a. The jets are formed with a small divergence angle and small cross-section later, as shown in Figure 3b and 3c at $t = 6$ ps and $t = 14$ ps, respectively. Meanwhile, some return electrons are generated, which induce the additional return current shown in Figure 3c and the additional inverse electric field shown in Figure 3e and 3f, which are not beneficial for the jet formation.

The IMF is simultaneously formed. Here the transverse IMF at $x = 0.25$ mm is shown in Figure 3g–3i. In Figure 3h and 3i, the toroidal IMF around the jet implies the collimation of the jet. The rotation direction of the transverse IMF in the outer toroid is opposite to that in the center shown in Figure 3i, which indicates the phenomenon of return current seen in Figure 3c. At the symmetric longitudinal positions of the plasma, the rotation directions of such transverse IMF are opposite and the strengths

are almost the same. These characteristics are in accordance with that of the IEF E_x . Therefore, the transverse IMF in the middle plane of the plasma is also close to zero.

The evolutions of the IEF and IMF with time have been verified at three different positions of the plasma. Within 2 ps, the IEF reaches high amplitudes, which is clearly illustrated in Figure 4a–4c. Moreover, the induced B_x , B_y , and B_z in Figure 4d–4f have trends similar to those of the induced E_x , E_y , and E_z , respectively, in spite of an approximate phase difference of π . Overall, the IMF and IEF oscillate strongly inside the plasma and weakly outside the plasma. After 2 ps, the amplitude of E_x gradually reduces with time. Especially at $x = 0.7$ mm (outside the plasma) shown in Figure 4a, E_x is always negative, which is beneficial for the acceleration of the electrons outside the plasma and the formation of the jets. More interestingly, the periodical oscillation of the IMF appears related to certain waves produced in the plasma, which is worthy of further study.

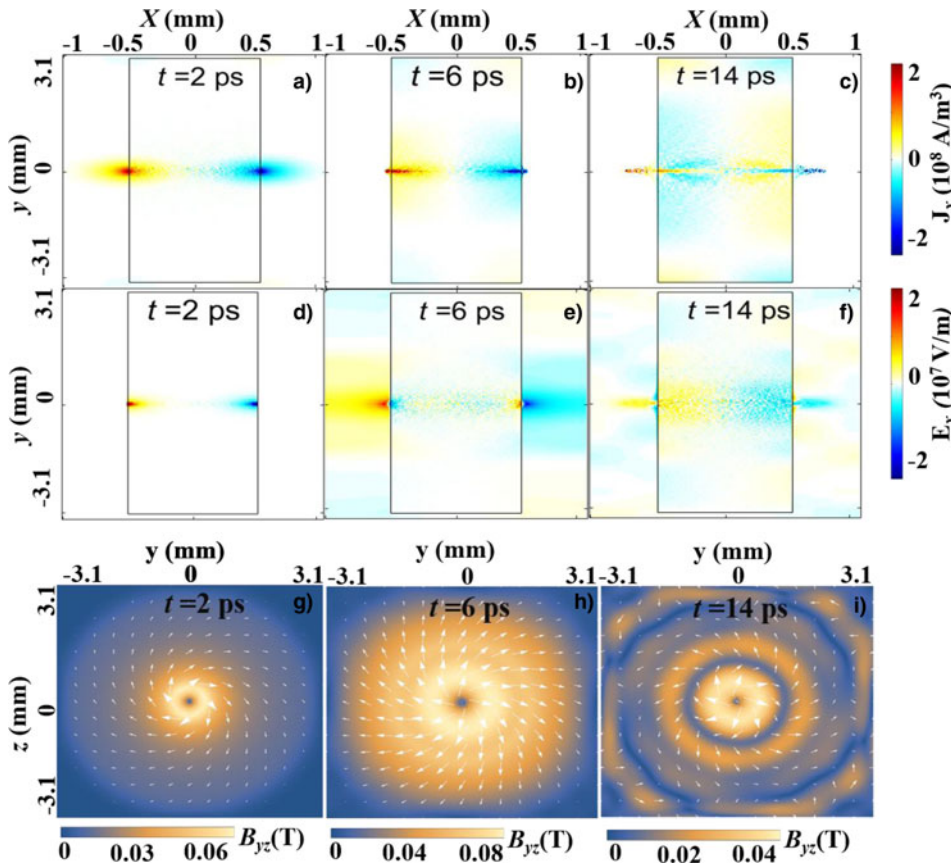


Fig. 3. Distribution of the longitudinal current density (first row) and the longitudinal IEF E_x (second row) in the xoy plane at time $t = 2$ ps in (a), (d), $t = 6$ ps in (b), (e), and $t = 14$ ps in (c), (f). The black rectangular box denotes the outline of the plasma in the xoy plane. The third row shows the distribution of transverse IMF in the yz plane at $x = 0.25$ mm (one-quarter of the longitudinal length of the plasma from $x = 0$ mm) at time $t = 2, 6, 14$ ps in (g), (h), and (i), respectively, where the blue-yellow scale in the background shows the strength of the transverse IMF and the superimposed white arrows indicate the transverse IMF vectors.

Explanation of electron jet formation

To check the effects of the IEF and IMF shown in Figure 3 on the jet formation, we focus on the dependence of electron ejection on the electric field. We divide the electric field into two components, $E_x \hat{x}$ and \vec{E}_\perp ($\vec{E}_\perp = E_y \hat{y} + E_z \hat{z}$), where \hat{y} and \hat{z} denote the unit vectors in the y and z directions, respectively. The equation of electron motion is $d\vec{p}^2/dt = 2eE_x p_x + 2e\vec{E}_\perp \times \vec{p}_\perp$, where $\vec{E}_\perp \times \vec{p}_\perp = E_y p_y \hat{z} + E_z p_z \hat{y}$. In addition, the energy of each electron is $\gamma^2 = 1 + (\vec{p}^2/m^2 c^2) = 1 + \Gamma_x + \Gamma_\perp$ (Gahn *et al.*, 1999). According to the position and momentum of all electrons in the PIC simulation, we calculate

$$\Gamma_x = \int_0^t \frac{2eE_x p_x}{(mc)^2} dt', \quad (2)$$

$$\Gamma_\perp = \int_0^t \frac{2e\vec{E}_\perp \times \vec{p}_\perp}{(mc)^2} dt', \quad (3)$$

where Γ_x is the longitudinal energy gain owing to the acceleration of the electric component $E_x \hat{x}$ (the IEF in the longitudinal direction), and Γ_\perp represents the transverse energy gain from \vec{E}_\perp (including the applied electrostatic field and transverse IEF). As shown in Figure 5a, the energy gain of the electron Γ_\perp is much larger than Γ_x at $t = 0.4$ ps when the electrons obtain longitudinal velocity and the jet is not formed clearly, as illustrated in Figure 5b. The electrons with energy gain Γ_\perp larger than Γ_x constitute 98.31% of the total electrons, which proves that the transverse electric field acceleration is the dominant acceleration mechanism.

Under the condition $p_x = 0$ and with no longitudinal force imposed on the electrons at $t = 0$ ps, it can be seen that the increments of p_\perp are converted into those of p_x through the effect of the transverse IMF (shown in Figure 3g–3i), that is, the $\vec{v}_\perp \times \vec{B}_\perp$ interaction. Therefore, the power source of the electrons ejecting from the plasma results from the transverse IMF, and the distribution of E_x (shown in Figure 3d–3f) clearly verifies the ejection of the jets in the opposite directions from the two ends of the cylindrical plasma, as shown in Figure 1.

In order to obtain larger longitudinal electron momentum P_x , we study the relationship between P_x and the applied electrostatic field shown in Figure 6. The jets can be formed when E_{\max} is in a wide range of $10^4 \sim 10^{12}$ V/m. As shown in Figure 6, we can find that the higher the applied electrostatic field is, the higher P_x is. Especially, when E_{\max} approaches 3×10^{10} V/m, the electron momentum P_x could reach $0.5m_e c$.

Considering that the strong electric and magnetic fields are difficult to be synchronously applied on the time scale of ps, two simulations with 2 ps delay of (1) the applied magnetostatic field and (2) the applied electrostatic field are carried out, respectively. For the former case (2 ps delay of the applied magnetostatic field), the electron jets achieve better collimation and higher intensity shown in Figure 7a–7c, compared with that with the electrostatic and magnetostatic fields applied on the plasma synchronously shown in Figure 3a–3c, respectively. It indicates that the plasma with directed transverse velocity is beneficial for the formation of the electron jets. Compared with another case of 2 ps delay of the electric field (only the applied magnetostatic field interacting with the cold plasma within 2 ps), the magnetostatic field makes no effect on the electron jets in 2 ps. As shown in Figure 7d–7f, the results of the simulation are almost the same

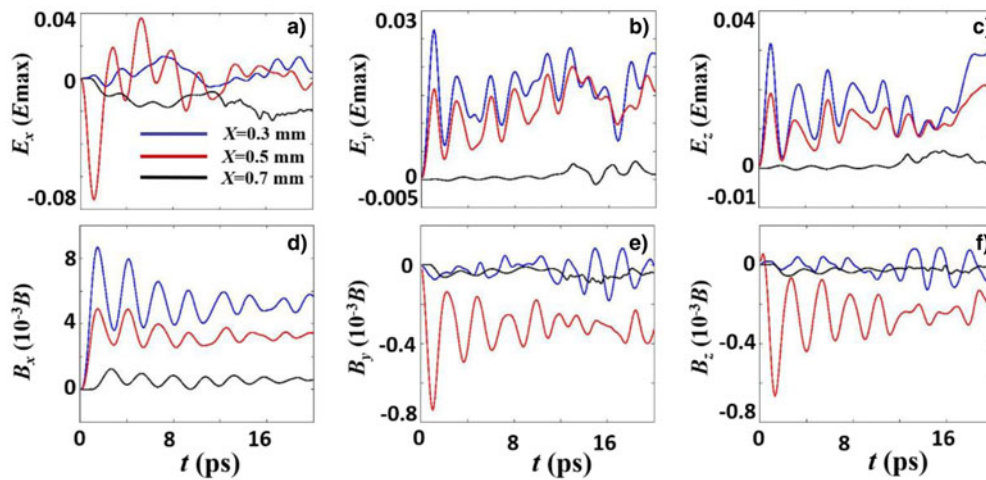


Fig. 4. Evolutions of (a–c) the IEF normalized to $E_{\max} = 3 \times 10^9$ V/m and (d–f) the IMF normalized to $10^{-3} B_0$ in (a, d) x, (b, e) y, and (c, f) z directions at different locations along the x-axis at $x=0.3$ mm (within the plasma), $x=0.5$ mm (on the top surface of the plasma), and $x=0.7$ mm (outside the plasma).

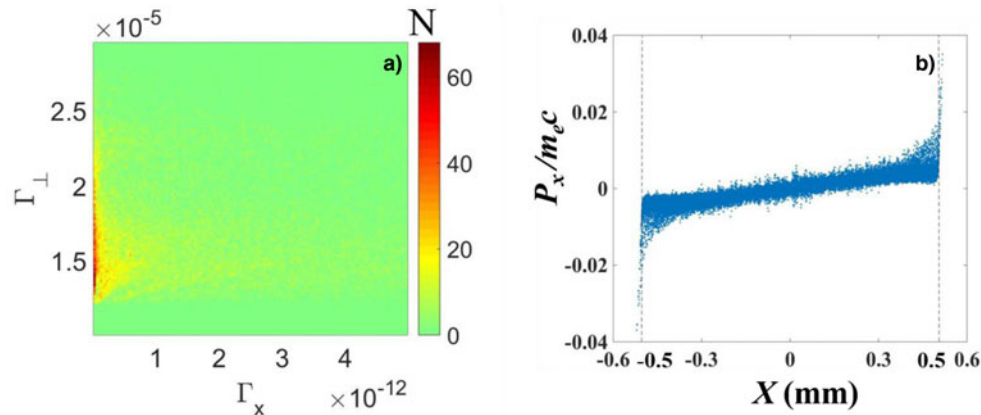


Fig. 5. (a) Distribution of the accelerated electrons in the energy gain space (Γ_x , Γ_{\perp}) at $t=0.4$ ps within the range $1.0 \times 10^{-17} < \Gamma_x < 5.0 \times 10^{-12}$ and $1.0 \times 10^{-5} < \Gamma_{\perp} < 3.0 \times 10^{-5}$ chosen for distinct display. The color bar represents the number of electrons (N). (b) Distribution of the longitudinal electron momentum P_x normalized to $m_e c$ within -0.2 mm $\leq y$, $z \leq 0.2$ mm at $t=0.4$ ps, where the dashed lines on the left and right denote the locations of $x=-0.5$ mm and $x=0.5$ mm, respectively.

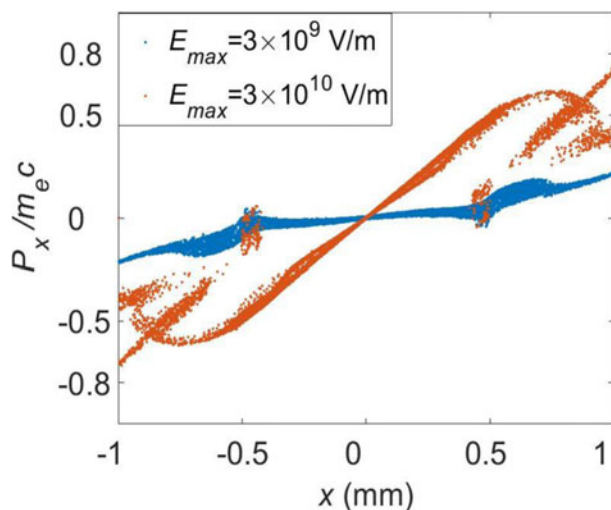


Fig. 6. Distribution of the longitudinal electron momentum P_x normalized to $m_e c$ within -0.074 mm $\leq y$, $z \leq 0.074$ mm (around the x-axis) at $t=20$ ps under different applied electrostatic fields.

as that in the proposed scheme (shown in Figure 3a–3c) except for 2 ps delay. All these results indicate that the applied electrostatic field play a significant role of the jet formation, and the applied magnetostatic field only contributes a lot on the collimation of the jets.

Based on the role of the electric and magnetic fields for the electron jet formation, a 2 ps delay of the applied magnetostatic field is set with the applied electrostatic field $E_{\max} = 3 \times 10^9$ V/m. The longitudinal electron momentum P_x could reach $0.7m_e c$ at $t=20$ ps as shown in online Supplementary Figure S3a, owing to the time delay of the applied magnetostatic field to great extent. The total charge of the ejected electrons (with energy above 10 keV) Q_e reaches $2 \times 10^{10} e$ at time around $t=8$ ps as shown in online Supplementary Figure S3b, and later keeps stable, which may be of great value for the stable and high total charge. The electron jets obtain good collimation at $t=20$ ps, shown in online Supplementary Figure S3c, which confirms the stability of the output of the total charge. If the parameters such as the plasma density are optimized, higher charge could be obtained.

In the above analysis, we showed that the collimated jets are formed when proper electric and magnetic fields are applied in

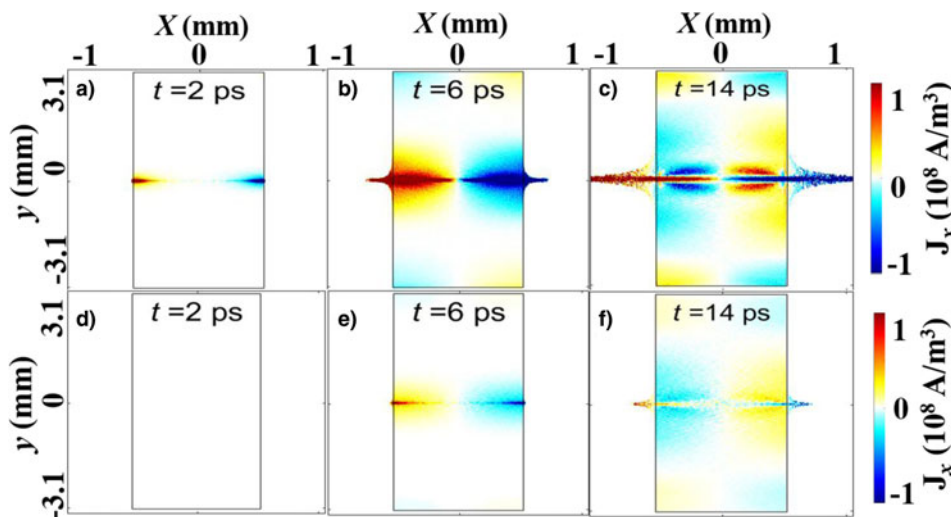


Fig. 7. Distribution of the longitudinal current density in the xoy plane at time $t = 2$ ps in (a), (d), $t = 6$ ps in (b), (e), and $t = 14$ ps in (c), (f). The black rectangular box denotes the outline of the plasma in the xoy plane. In the first row (a)–(c), 2 ps delay of the applied magnetostatic field. In the second row (d)–(f), 2 ps delay of the electrostatic field.

the cylindrical plasma. We also notice that in the active galactic nuclei (AGN) jet (Marscher, 2006; Zhai *et al.*, 2014), the density is approximately 10^3 m^{-3} and the length is in the 10^{20} m scale. According to the scaling law of the particle motion equations of the system, the voltage and magnetic fields in the celestial bodies should be 10^{18} V and 10^{-8} – 10^{-9} T , respectively, for similar jets to be formed. These values are reasonable, as the voltage is $1.1 \times 10^{18} \text{ V}$ and the magnetic field is $2 \times 10^{-9} \text{ T}$ in the AGN jet. Owing to this set of parameters being consistent with that of electric and magnetic fields in the celestial bodies, our model may provide theoretical explanations for the jet formation in the celestial bodies (Stehle *et al.*, 2009) to some extent.

Conclusions

In conclusion, the electrons gather into the center of the plasma spirally and collectively under the condition of proper applied electrostatic and magnetostatic fields. Initially, the transverse electric field acceleration is the dominant acceleration mechanism. Meanwhile, the transverse energy of the electrons is converted into the longitudinal energy via the effect of the transverse IMF. The electrons gain longitudinal momentum, thus forming the jets. The longitudinal electron momentum varies considerably under different applied electrostatic fields. Notably, the maximum velocity of electrons is close to the speed of light when the maximum applied radial electrostatic field reaches $3 \times 10^{10} \text{ V/m}$. Based on the scaling law, the jets observed in the celestial bodies can be explained by our model to some extent, as the electric and magnetic fields in the celestial bodies are similar to the conditions in our model.

Supplementary material. The supplementary material for this article can be found at <https://doi.org/10.1017/S0263034618000381>.

Acknowledgments. This work is supported by the National Natural Science Foundation of China (Grant No. 11335013, 11374319, 11575274, 11127901, and 11674339), the Ministry of Science and Technology of the People's Republic of China (Grant No. 2016YFA0401102), and the Strategic Priority Research Program of the Chinese Academy of Sciences (Grant No. XDB16).

References

Albert F, Thomas AGR, Mangles SPD, Banerjee S, Corde S, Flacco A, Litos M, Neely D, Vieira J, Najmudin Z, Bingham R, Joshi C and

- Katsouleas T (2014) Laser wakefield accelerator based light sources: potential applications and requirements. *Plasma Physics and Controlled Fusion* **56**, 084015 (1–10).
- Baker DA, Hammel JE and Ribe FL (1961) Rotating plasma experiments. I. Hydromagnetic properties. *The Physics of Fluids* **4**, 1534–1548.
- Bridle AH (1986) Extragalactic jets: trends and correlations. *Canadian Journal of Physics* **64**, 353–361.
- Chen LM, Park JJ, Hong KH, Kim JL, Zhang J and Nam CH (2002) Emission of a hot electron jet from intense femtosecond-laser-cluster interactions. *Physical Review E* **66**, 025402 (1–4).
- Fahleson UV (1961) Experiments with plasma moving through neutral gas. *The Physics of Fluids* **4**, 123–127.
- Gahn C, Tsakiris GD, Pukhov A, Meyer-ter-Vehn J, Pretzler G, Thiroff P, Habs D and Witte KJ (1999) Multi-MeV electron beam generation by direct laser acceleration in high-density plasma channels. *Physical Review Letters* **83**, 4772–4775.
- Haines MG (2011) A review of the dense Z-pinch. *Plasma Physics and Controlled Fusion* **53**, 093001 (1–168).
- Hu G-y, Lei A-l, Wang W-t, Wang X, Huang L-g, Wang J-w, Xu Y, Liu J-s, Yu W, Shen B-f, Li R-x and Xu Z-z (2010) Collimated hot electron jets generated from subwavelength grating targets irradiated by intense short-pulse laser. *Physics of Plasmas* **17**, 033109 (1–4).
- Kang N, Lin Z, Shen B, Liu H, Lei A, Fan W, Zhou S and Wang L (2016) Two-dimensional particle-in-cell simulation of small-scale laser-plasma interactions with laser-produced plasma jets. *Journal of the Optical Society of America B* **33**, 932–941.
- Kasperczuk A, Paduch M, Tomaszewski K, Zielinska E, Miklaszewski R and Szymaszek A (2016) A plasma focus device as a metallic plasma jet generator. *Laser and Particle Beams* **34**, 356–361.
- Kasperczuk A, Paduch M, Tomaszewski K, Miklaszewski R, Jach K, Swierczynski R, Szymaszek W, Zielinska E and Szymaszek A (2017) Optimization of parameters of a copper plasma jet produced at the plasma focus device. *Laser and Particle Beams* **35**, 561–568.
- Katsouleas T and Dawson JM (1983) Unlimited electron acceleration in laser-driven plasma waves. *Physical Review Letters* **51**, 392–395.
- Lehnert B (1971) Rotating plasmas. *Nuclear Fusion* **11**, 485–533.
- Marscher AP (2006) Relativistic jets in active galactic nuclei. *AIP Conference Proceedings* **856**, 1–22.
- Nakajima K, Fisher D, Kawakubo T, Nakanishi H, Ogata A, Kato Y, Kitagawa Y, Kodama R, Mima K, Shiraga H, Suzuki K, Yamakawa K, Zhang T, Sakawa Y, Shoji T, Nishida Y, Yugami N, Downer M and Tajima T (1995) Observation of ultrahigh gradient electron acceleration by a self-modulated intense short laser pulse. *Physical Review Letters* **74**, 4428–4431.
- Nakajima K, Deng A, Zhang X, Shen B, Liu J, Li R, Xu Z, Ostermayr T, Petrovics S, Klier C, Iqbal K, Ruhl H and Tajima T (2011) Operating plasma density issues on large-scale laser-plasma accelerators toward high-energy frontier. *Physical Review Special Topics – Accelerators and Beams* **14**, 091301 (1–12).

- Nakajima K, Kim HT, Jeong TM and Nam CH** (2015) Scaling and design of high-energy laser plasma electron acceleration. *High Power Laser Science and Engineering* **3**, e10 (1–11).
- Nieter C and Cary JR** (2004) VORPAL: a versatile plasma simulation code. *Journal of Computational Physics* **196**, 448–473.
- Salamin YI and Keitel CH** (2002) Electron acceleration by a tightly focused laser beam. *Physical Review Letters* **88**, 095005 (1–4).
- Salehi F, Goers AG, Hine GA, Feder L, Kuk D, Miao B, Woodbury D, Kim KY and Milchberg HM** (2017) MeV electron acceleration at 1 kHz with <10 mJ laser pulses. *Frontiers in Optics* **42**, 215–218.
- Shaw JL, Tsung FS, Vafaei-Najafabadi N, Marsh KA, Lemos N, Mori WB and Joshi C** (2014) Role of direct laser acceleration in energy gained by electrons in a laser wakefield accelerator with ionization injection. *Plasma Physics and Controlled Fusion* **56**, 84006–84012.
- Shaw JL, Lemos N, Amorim LD, Vafaei-Najafabadi N, Marsh KA, Tsung FS, Mori WB and Joshi C** (2017) Role of direct laser acceleration of electrons in a laser wakefield accelerator with ionization injection. *Physical Review Letters* **118**, 064801 (1–5).
- Sprangle P, Esarey E and Krall J** (1996) Laser driven electron acceleration in vacuum, gases, and plasmas. *Physics of Plasmas* **3**, 2183–2190.
- Stehle C, Ciardi A, Colombier JP, Gonzalez M, Lanz T, Marocchino A, Kozlova M and Rus B** (2009) Scaling stellar jets to the laboratory: the power of simulations. *27*, 709–717.
- Ting A, Moore CI, Krushelnick K, Manka C, Esarey E, Sprangle P, Hubbard R, Burris HR, Fischer R and Baine M** (1997) Plasma wakefield generation and electron acceleration in a self-modulated laser wakefield accelerator experiment. *Physics of Plasmas* **4**, 1889–1899.
- Wagner R, Chen SY, Maksimchuk A and Umstadter D** (1997) Electron acceleration by a laser wakefield in a relativistically self-guided channel. *Physical Review Letters* **78**, 3125–3128.
- Wang F-L, Pei X-X, Han B, Wei H-G, Yuan D-W, Liang G-Y, Zhao G, Zhong J-Y, Zhang Z, Zhu B-J, Li Y-F, Li F, Li Y-T, Zeng S-L, Zou S-Y and Zhang J** (2016) Laboratory astrophysics with laser-driven strong magnetic fields in China. *High Power Laser Science and Engineering* **4**, e27 (1–4).
- Wilcox JM** (1959) Review of high-temperature rotating-plasma experiments. *Reviews of Modern Physics* **31**, 1045–1051.
- Woodbury DC, Feder L, Shumakova V, Gollner C, Miao B, Schwartz R, Baltuška A, Pugzlys A and Milchberg H** (2018) Laser wakefield acceleration with mid-IR laser pulses. *Optics Letters* **43**, 1131–1134.
- Yu W, Bychenkov V, Sentoku Y, Yu MY, Sheng ZM and Mima K** (2000) Electron acceleration by a short relativistic laser pulse at the front of solid targets. *Physical Review Letters* **85**, 570–573.
- Yu TP, Yu W, Shao FQ, Luan SX, Zou DB, Ge ZY, Zhang GB, Wang JW, Wang WQ, Li XH, Liu JX, Ouyang JM and Wong AY** (2015) High-energy-density electron jet generation from an opening gold cone filled with near-critical-density plasma. *Journal of Applied Physics* **117**, 023105 (1–6).
- Zhang X, Shen B, Ji L, Wang W, Xu J, Yu Y, Yi L, Wang X, Hafz NAM and Kulagin V** (2012) Effect of pulse profile and chirp on a laser wakefield generation. *Physics of Plasmas* **19**, 053103 (1–7).
- Zhai X, Li H, Bellan PM and Li ST** (2014) Three-dimensional MHD simulation of the Caltech plasma jet experiment: first results. *The Astrophysical Journal* **791**, 40 (1–22).